RSC Advances

PAPER

View Article Online
View Journal | View Issue

Cite this: *RSC Adv.*, 2021, **11**, 38804

Ferrocene donor linked to pyridine/pyridinium acceptor *via* a systematically enlarged π-linker†

Jiří Kulhánek,[a] Milan Klikar,[a] Oldřich Pytela,[a] Zdenka Růžičková[b] and Filip Bureš *[a]

Received 8th November 2021
Accepted 26th November 2021

DOI: 10.1039/d1ra08186a

rsc.li/rsc-advances

Nine chromophores with ferrocene donor and pyridine/pyridinium acceptors have been prepared and further investigated. The performed X-ray analysis showed partially polarized and geometrically oblate pyridine unit. An extension of the π-system and *N*-quaternization were revealed as suitable tools for exclusive manipulation of the LUMO with the almost steady HOMO. Whereas the electrochemical HOMO–LUMO gap can be tuned from 3.01 to 1.49 eV, the high- and low-energy absorption bands were found within the range of 280–402/456–547 nm. The pyridinium chromophores showed distinct negative solvatochromism. A thorough DFT analysis has been performed; it turned out that ferrocene donor is capable of two principal D–A interactions, whose employment depends on the appended electron-withdrawing moiety.

Introduction

Due to their D–π–A arrangement (D = donor, π = conjugated system and A = acceptor), organic push–pull molecules represent a unique class of organic π-conjugated systems.[1] A direct electron communication between the D and A parts called intramolecular charge-transfer (ICT) imparts push–pull molecules distinct properties such as dipolar structure, optical properties and colour, supramolecular arrangement, conductivity, solubility *etc.* Moreover, the ICT in organic D–π–A molecules is tuneable within a broad range, which allows tailoring their properties towards particular applications across organic electronics and photonics. Push–pull molecules are commonly found as active substances of organic light-emitting diodes (OLED),[2] organic field-effect transistors (OFET),[3] organic photovoltaic cells (OPVC)[4] and dye-sensitized solar cells (DSSC).[5] Due to their dipolar and polarizable structure, organic push–pull chromophores found also numerous applications across nonlinear optics (NLO).[1,6]

In contrast to inorganic systems, organic D–π–A molecules with well-defined structure are often easy to synthesize and processed/engineered. In principle, their property tuning involves modification of D, π and A parts as well as their overall arrangement.[7] Whereas electron releasing D part is commonly introduced by appending groups with positive electronic effects (+I and +M; *e.g.* dialkylamino/alkoxy groups), electron withdrawing groups possess opposite effects (*e.g.* cyano/nitro groups). In addition to these common donors and acceptors, complex heterocyclic units such as proaromatic pyranylidene, thienothiophenes, carbazole and dicyanovinyl, dicyanoimidazole, tricyanofuran, indandione, (thio)barbituric acid, ThDione, *etc.* were also widely employed in push–pull molecules.[7,8] The π-system involves multiple bonds, aromatic and heterocyclic units and their combinations.

Metallocenes, ferrocene (Fc) in particular, are electron-rich moieties employed as donors in push–pull chromophores.[9] The electroactive ferrocene incorporated into a push–pull molecule brings defined redox process,[10] chromophore nonplanarity[11] and enhanced thermal stability.[12] On the contrary, six-membered pyridine (Py) belongs to electron poor heterocycles, which may be utilized as an electron acceptor.[1,13] A mutual conjugated interconnection of Fc and Py moieties renders a push–pull system. Fc–π–Py molecules were widely utilized as tailored ligands chelating (transition) metals.[14] The resulting complexes often showed cytotoxicity or distinct electrochemical sensing towards metal cations.

Various dyes, mostly in push–pull arrangement, were constructed from the Fc and Py moieties.[15] Many of them showed very interesting and pronounced NLO properties.[16] Very nice example of a functionalized Fc-derivative with two linked Py-pendants, featuring photoelectric properties adjustable by pH, has recently been reported by Shi *et al.*[17] In 2013, ferrocene electron donor has been utilized for the construction of push–pull dyes also in our laboratory.[18]

In order to extend these studies and in view of the pyridine facile quaternization capability,[15a,19] we report herein Fc-derived push–pull molecules with pyridyl (Py) and pyridinium (Py^+)

[a]*Institute of Organic Chemistry and Technology, Faculty of Chemical Technology, University of Pardubice, Studentská 573, Pardubice, 53210, Czech Republic. E-mail: filip.bures@upce.cz*

[b]*Department of General and Inorganic Chemistry, Faculty of Chemical Technology, University of Pardubice, Studentská 573, Pardubice, 53210, Czech Republic*

† Electronic supplementary information (ESI) available: Further synthetic details, RTG, electrochemical and optical data, DFT results, NMR spectra. CCDC 2110542 and 2110543. For ESI and crystallographic data in CIF or other electronic format see DOI: 10.1039/d1ra08186a

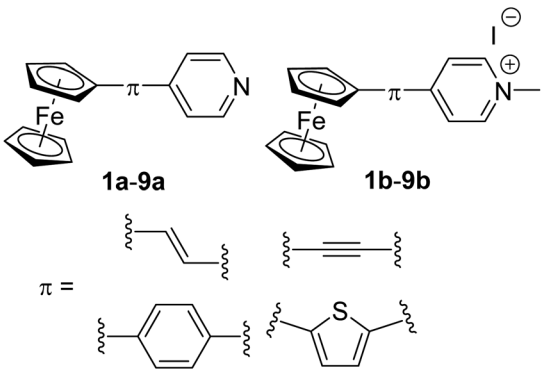

Fig. 1 General structure of investigated Fc–π–Py and Fc–π–Py$^+$ push–pull chromophores.

acceptors (Fig. 1). Besides employing two related Py/Py$^+$ acceptors, further property tuning has been achieved by altering the π-conjugated pathway.

Results and discussion

Synthesis

The synthesis of pyridine (**a**) and pyridinium (**b**) chromophores **1–9** involved preparation of Fc–π–Py compounds and their subsequent quaternization using iodomethane. The synthesis of compounds **1a–9a** utilized three cross-coupling reactions as outlined in Scheme 1. Compounds **1a** and **9a** were prepared using ferroceneboronic acid and commercially available 4-iodopyridine **16** and intermediate **17** (see the ESI† for its synthesis). Similar Suzuki–Miyaura reaction[14c] between commercial pyridin-4-ylboronic acid **11** and precursors **18** (see the ESI†) or **19** (ref. 18*b*) has also been employed for the construction of compounds **4a** and **7a**. Heck olefination[18a] between vinylferrocene **12** or 4-vinylpyridine **13** with 4-iodopyridine **16** and precursors **18** and **19** afforded target Fc–π–Py chromophores **2a** (61%), **5a** (53%) and **8a** (64%). A modified procedure for Sonogashira reaction[18a] has been employed for preparation of compounds **3a** and **6a**. Commercially available ethynylferrocene **14** and precursor **16** afforded **3a** in 68% yield, while chromophore **6a** was prepared by reacting 4-ethynylpyridine hydrochloride **15** with **18**. The pyridinium salts **1b–9b** were gained by reacting **1a–9a** with boiling iodomethane in the yield ranging between 83 and 98% (Scheme 1).

X-ray analysis

A slow evaporation of dichloromethane solutions of compounds **6a** and **7a** provided mono-crystals suitable for X-ray analysis, see the ESI† for complete details. The plots shown in Fig. 2 confirm their molecular structure and the solid-state arrangement. Their structures are composed of almost coplanar arrangement of the ferrocene Cp ring and the appended π-system with diminished interplanar angles ranging from 0.5 to 12°. The extent of the ICT in **6a** and **7a** may be assessed by calculating bond-length alternation of the particular π-system. Using Bird index (I_6/I_5),[20] the indexes I_6/I_5 of unsubstituted benzene/thiophene are 100 and 66, respectively. The experimental values obtained for 1,4-phenylene (92.8) and 2,5-thienylene (60.5) moieties in **6a** and **7a** imply that both molecules are polarized and partially adopt quinoid character. Moreover, thiophene polarization in **6a** is not far from that observed for T-shaped chromophores (I_5 ~58) featuring very efficient ICT.[21] On the contrary, the I_6 values of the terminal pyridine rings (94.3 and 91.6) are higher than expected for unsubstituted pyridine (I_6 = 85.7). However, when employing harmonic oscillator model of aromaticity (HOMA),[22] the obtained values **6a** and **7a** are 0.875 and 0.897, while unsubstituted pyridine possesses the HOMA within the range of 0.944–1 (based on the source data). Hence, the pyridine rings in **6a**/**7a** are considered as partially polarized and geometrically oblate with the shortest C–N bonds (1.33–1.39 Å). The supramolecular arrangement of **6a** revealed two-component inversion twin.

Electrochemistry

The electrochemical characteristics of pyridine derivatives **1a–9a** as well as pyridinium salts **1b–9b** were investigated in acetonitrile containing 0.1 M Bu_4NPF_6 in a three-electrode cell by cyclic voltammetry (CV). The acquired data are summarized in Table 1, see the ESI† for a complete list of CV diagrams (Fig. S7–12†).

Push–pull character of Fc–π–Py chromophores **1a–9a** implies that the first oxidation most likely takes place on the ferrocene donor, while the first reduction involves the pyridine acceptor and adjacent π-linker. Due to ferrocene presence, the first oxidation was always determined as reversible process with peak-to-peak separation within the 60–80 mV implying one-electron transfer. On the other hand, the first reductions were recorded as irreversible or quasi-reversible processes followed by subsequent reductions with more negative potentials. As compared to $i_{pa(ox1)}$ values, the first reductions possess two/three times higher cathodic peak current $i_{pc(red1)}$, which corresponds to the two-electron reduction; three electron reductions were recorded for acetylene derivatives **3a**, **6a** and **9a**. A precedent reduction process, seen as a shoulder accompanying the anodic peak of the ferrocene oxidation, has been observed for compounds bearing double/triple bonds. The peak potentials of the first oxidation/reduction $E_{p(ox1/red1)}$ were recalculated to energies of the HOMO and LUMO ($E_{HOMO/LUMO}$) (Table 1). These were further visualized in the energy level diagram shown in Fig. 3.

When going from **1a** to **9a**, the HOMO remained almost unaltered and principal changes are seen in the LUMO level. With the same donor and acceptor, these changes reflect composition of the π-linker. In chromophore threesomes **1a–3a**, **4a–6a** and **7a–9a**, the lowest LUMO (and also the HOMO–LUMO gap ΔE) was recorded for compounds **2a**, **5a** and **8a** bearing olefinic subunit. This is mostly due to its ICT transparency and planarization effect.[1] When going from **4a–6a** to **7a–9a**, the latter showed narrowed ΔE, which obeys our comparison of 1,4-phenylene and 2,5-thienylene moieties embedded in push–pull molecules.[23] Hence, by gradually

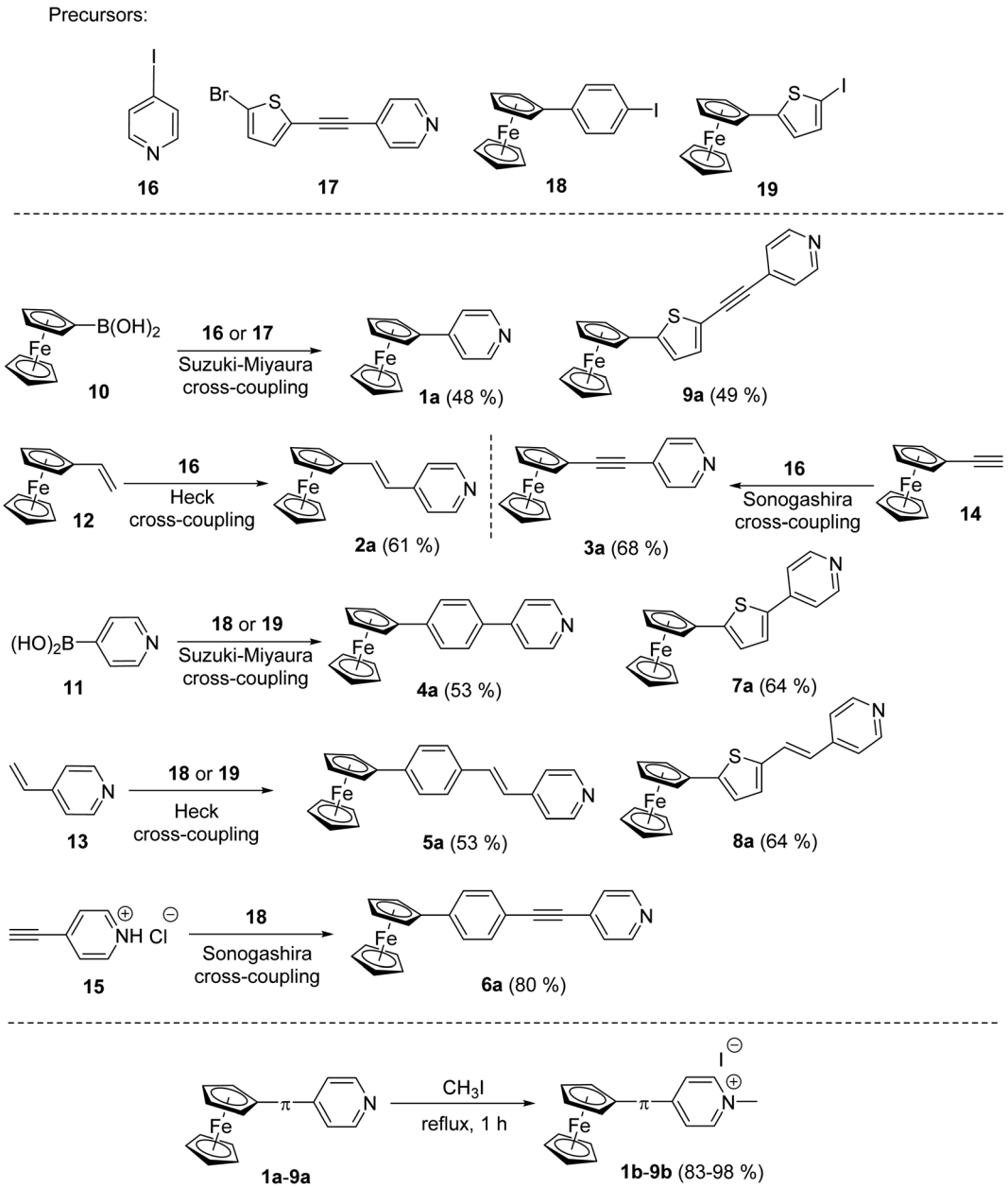

Scheme 1 Synthetic strategy towards Fc–π–Py push–pull chromophores **1a–9a** with systematically enlarged π-system and their subsequent *N*-quaternization to **1b–9b**.

extending the π-system (**1a** → **8a**), the HOMO–LUMO gap may be tuned from 3.01 to 2.36 eV.

Electrochemical investigation of Fc–π–Py^+ chromophores **1b–9b** revealed additional $I^- \rightarrow I_3^-$ oxidation located at around +400 mV appearing as a single wave (**1b–3b** and **7b–9b**) or shoulder accompanying Fc redox process (**4b–6b**). In order to properly distinguish both redox processes, a joint CV diagram of representative compound **1b** with its analogue quaternized by dimethylsulfate (containing electrochemically inactive $MeOSO_3^-$ anion instead of I^-) along with the electrochemical oxidation of I^- (KI) is provided in the ESI (Fig. S13†). As can be seen from the energy level diagram in Fig. 3, the HOMO levels of pyridiniums **1b–9b** remained almost unaltered as compared to the original pyridines **1a–9a**. *N*-Quaternization significantly affected the LUMO levels that generally dropped by ~1 eV.

Moreover, a combination of the pyridinium acceptor along with electronegative acetylenic unit (as in **6b** and **9b**) bring the lowest HOMO–LUMO gap of 1.49 and 1.50 eV. This is in contrast to aforementioned pyridine series **a** in which the lowest ΔE has been recorded for olefinic chromophores. Overall, by varying the π-system and *via N*-quaternization, the HOMO–LUMO gap in **1–9** may be tuned within the broad range of 3.01 to 1.49 eV.

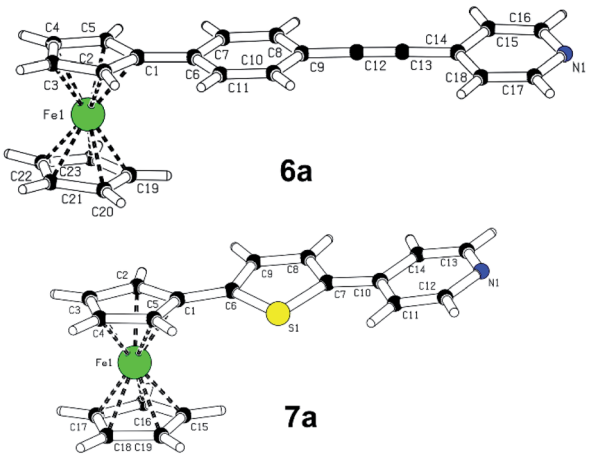

Fig. 2 X-ray molecular representation of chromophore **6a** (CCDC 2110543) and **7a** (CCDC 2110542).

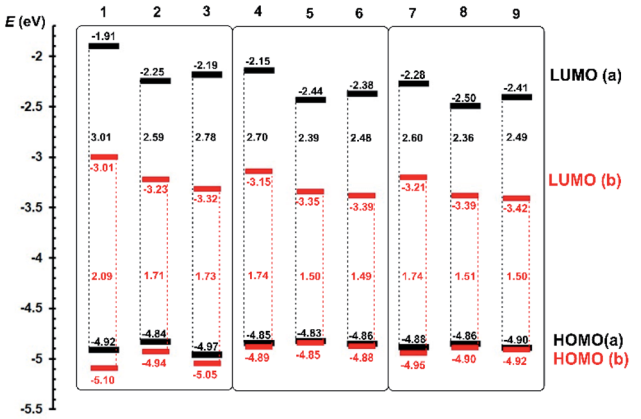

Fig. 3 Energy level diagram of electrochemically determined HOMO and LUMO levels for Fc–π–Py (black) and Fc–π–Py$^+$ (red) chromophores **1a–9a** and **1b–9b**.

Electronic absorption spectra

All Fc–π–Py and Fc–π–Py$^+$ derivatives **1–9** are intensively coloured compounds. Their colour ranges from orange to dark red, while none emissive properties were observed. Table 1 lists the longest wavelength absorption maxima and the corresponding molar absorption coefficients and Fig. 4 shows absorption spectra of representative chromophores in acetonitrile (ACN); see the ESI† for complete spectra. For Fc-derivatives, two electronic transitions and two particularly developed bands are generally seen.[18,26] Whereas the low-energy (LE) band corresponds to the transition from the Fe-centred HOMO to the LUMO, the high-energy (HE) band originates from the interaction of the Cp/π-localized HOMO−3 and the LUMO. According to this model, an extension of the π-system should primarily affect the position of the HE band. Indeed, when comparing the λ_{max} values of the HE and LE bands listed in Table 1, the principal changes are seen in the position of the HE band ($\Delta\lambda^{HE}_{max}$ is 86 and 113 nm for Fc–π–Py and Fc–π–Py$^+$ chromophores). When going from parent **1a**/**1b** and gradually extending and varying the π-system, the HE band shifted from 280/313 to 366/426 nm of **8a**/**8b** bearing polarizable and planarized ethenylthiophene π-linker (Fig. 4a). On the contrary, variation in the λ^{LE}_{max} is rather low (8/48 nm within the series **a** and **b**). Upon *N*-quaternization (**a** → **b**), both HE and LE bands

Table 1 Experimentally obtained electrochemical and optical parameters of chromophores **1a–9a** and **1b–9b**

Comp.	$E_{pa(ox1)}$ [a] [V]	$E_{pc(ox1)}$ [a] [V]	$E_{1/2(ox1)}$ [b] [V]	$E_{pc(red1)}$ [a] [V]	$E_{pa(red1)}$ [a] [V]	$E_{1/2(red1)}$ [b] [V]	ΔE [d] [eV]	E_{HOMO} [e] [eV]	E_{LUMO} [e] [eV]	λ^{HE}_{max} [nm (eV)]/ ε ($\times10^3$)[f] [M^{-1} cm^{-1}]	λ^{LE}_{max} [nm (eV)]/ ε ($\times10^3$)[f] [M^{-1} cm^{-1}]
1a	0.45	0.38	0.42	−2.56	[c]	—	3.01	−4.92	−1.91	280 (4.43)/10.5	456 (2.72)/0.6
2a	0.37	0.30	0.34	−2.22	[c]	—	2.59	−4.84	−2.25	312 (3.97)/22.8	461 (2.69)/1.9
3a	0.5	0.42	0.46	−2.28	[c]	—	2.78	−4.97	−2.19	303 (4.09)/15.5	457 (2.71)/1.1
4a	0.38	0.32	0.35	−2.32	[c]	—	2.70	−4.85	−2.15	300 (4.13)/23.3	460 (2.70)/1.3
5a	0.36	0.29	0.33	−2.03	[c]	—	2.39	−4.83	−2.44	331 (3.75)/34.5	457 (2.71)/2.5
6a	0.39	0.32	0.36	−2.09	[c]	—	2.48	−4.86	−2.38	317 (3.91)/32.7	460 (2.70)/2.0
7a	0.41	0.33	0.37	−2.19	−2.04	−2.12	2.60	−4.88	−2.28	336 (3.69)/19.3	460 (2.70)/2.0
8a	0.39	0.31	0.35	−1.97	−1.86	−1.92	2.36	−4.86	−2.50	366 (3.39)/29.2	462 (2.68)/4.3
9a	0.43	0.35	0.39	−2.06	−1.91	−1.99	2.49	−4.90	−2.41	345 (3.59)/25.9	464 (2.67)/3.0
1b	0.63	0.55	0.59	−1.46	−1.37	−1.415	2.09	−5.10	−3.01	313 (3.96)/15.9	525 (2.36)/2.7
2b	0.47	0.4	0.435	−1.24	[c]	—	1.71	−4.94	−3.23	361 (3.43)/25.1	547 (2.27)/6.3
3b	0.58	0.5	0.54	−1.15	[c]	—	1.73	−5.05	−3.32	343 (3.62)/20.1	531 (2.34)/5.1
4b	0.42	0.35	0.385	−1.32	−1.24	−1.28	1.74	−4.89	−3.15	344 (3.60)/22.2	501 (2.48)/4.1
5b	0.38	0.31	0.345	−1.12	[c]	—	1.5	−4.85	−3.35	378 (3.28)/33.9	508 (2.44)/7.2
6b	0.41	0.35	0.38	−1.08	[c]	—	1.49	−4.88	−3.39	362 (3.43)/29.7	504 (2.46)/5.8
7b	0.48	0.41	0.445	−1.26	−1.18	−1.22	1.74	−4.95	−3.21	390 (3.18)/22.6	537 (2.31)/6.2
8b	0.43	0.36	0.395	−1.08	[c]	—	1.51	−4.90	−3.39	426 (2.91)/32.3	532 (2.33)/11.6
9b	0.45	0.39	0.42	−1.05	[c]	—	1.5	−4.92	−3.42	402 (3.08)/24.7	523 (2.37)/8.0

[a] $E_{pa/c(ox1)}$ and $E_{pa/c(red1)}$ are anodic or cathodic peak potentials of the first oxidation and reduction, respectively, measured by CV at scan rate 100 mV × s^{-1}; all potentials are given *vs.* SSCE (ACN). [b] $E_{1/2(ox1)}$ and $E_{1/2(red1)}$ are half-wave potentials of the first oxidation and reduction, respectively, for reversible or quasi-reversible processes; $E_{1/2(ox1/red1)} \approx (E_{pa(ox1/red1)} + E_{pc(ox1/red1)})/2$. [c] Irreversible first reductions. [d] $\Delta E = E_{pa(ox1)} - E_{pc(red1)}$. [e] $-E_{HOMO/LUMO} = (E_{pa(ox1)} + 0.036)$ or $(E_{pc(red1)} + 0.036) + 4.429$ (*vs.* SCE).[24] The increment of +0.036 V corresponds to the difference between SCE (0.241 *vs.* SHE) and SSCE (0.205 *vs.* SHE).[25] [f] Measured in ACN.

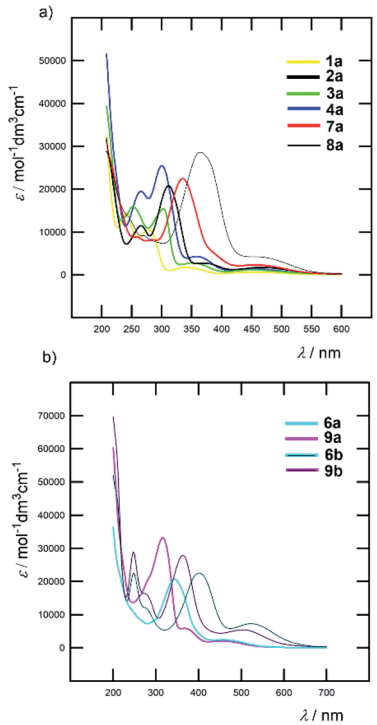

Fig. 4 Effect of π-system extension (a) and *N*-quaternization (b) on optical properties of selected Fc–π–Py and Fc–π–Py$^+$ chromophores (ACN).

shifted bathochromically by 30–60 and 70–90 nm, respectively. The *N*-quaternization affected the position of the LE band more significantly; see Fig. 4b for representative examples.

Besides acetonitrile, the spectra of pyridine chromophores were also recorded in dichloromethane (DCM). An inspection of the λ_{max} values gathered in Table S3† revealed that the solvatochromic behaviour of **1a–9a** is diminished with the $\Delta\lambda^{HE/LE}_{max}$ of 1–3/1–14 nm. On the contrary, the ionic Fc–π–Py$^+$ chromophores **1b–9b** showed hypsochromically-shifted HE and LE bands with increasing polarity of the solvent (Table S3†). For instance, the HE/LE bands of chromophore **8b** shifted from 455/558 to 426/532 and 432/437 nm when going from DCM to ACN and MeOH, respectively. This negative solvatochromism, a typical feature of pyridinium salts,[27] indicates that the excited state of Fc–π–Py$^+$ chromophores (**b**) is less polar as compared to the ground state.

DFT analysis

Pyridine as well as pyridinium derivatives **1–9** were theoretically investigated at the DFT level by using the Gaussian® 16 software package.[28] Their geometries were optimized using the DFT B3LYP/6-311+G(2df,p) method; energies of the frontier molecular orbitals and ground-state dipole moments μ were calculated using DFT B3LYP/6-311+G(2df,p) level with acetonitrile as solvent. First hyperpolarizabilities β were calculated using DFT B3LYP/6-311+G(2df,p) method in vacuum at 1064 nm. The electronic absorption spectra and the corresponding longest-wavelength absorption maxima and electron transitions were gained by TD-DFT B3LYP/6-311+G(2df,p) ($n_{states} = 8$) method. All calculated data are gathered in Table 2.

Relatively weak correlations have been found for the DFT-calculated and electrochemically-derived energies of the HOMO (Fig. S16 and S18†), which implies that the redox process, and subsequently also the ICT, are not solely dominated by a transition from the HOMO. This observation agrees with the aforementioned theory on multiple interaction of the ferrocene donor. On the contrary, the LUMO energies showed tight correlations (Fig. S17 and S19†), which means that the acceptor-centred LUMO is directly involved in the redox process and the ICT. Hence, the DFT-calculated LUMO energies obey the same trends as seen for the electrochemical E_{LUMO} values. A visualization of the frontier molecular orbitals (HOMO → HOMO−4 and LUMO → LUMO+4) are provided for the particular chromophore in Fig. S20–S37.† Except for acetylenic compounds **3b**, the HOMO and HOMO−1 are solely localized on the ferrocene Fe atom. On the contrary, the HOMO−2 is distributed further on the ferrocene Cp ring(s) and may also involve the appended π-system.

Surprisingly and in contrast to the aforementioned theory, the HOMO−3 mostly occupies the ferrocene Fe atom with a minimal distribution on the Cp ring(s). The HOMO−4 is spread over the whole Fc moiety and the appended π-system. The LUMO is localized either on the pyridine/pyridinium acceptor or on the appended π-linker. The higher vacant orbitals are variously distributed over the whole π-system including the ferrocene Cp ring. As expected, variation in the calculated ground state dipole moment within the series **a** is minimal (4.6–6.5 D), which reflects only extension of the π-system. However, upon *N*-quaternization, the dipole moment has significantly raised to 12.5–29.7 D, which is due to ionic nature of the pyridinium acceptor including bulky I^- anion in compounds **b**.

The calculated electronic absorption spectra along with the spectra recorded in ACN are shown in Fig. S38 and 39,† while the longest-wavelength absorption maxima are listed in Table 2. As compared to the experimental data, the calculated spectra are slightly bathochromically shifted but possess the same features and bands. The spectra of chromophores **1a**, **3a** and **4a** with short, less polarizable or nonplanar π-linker possess diminished LE band. An analysis of the transitions forming these bands revealed close to zero oscillator strengths. The remaining Fc–π–Py chromophores possess both bands. The LE bands are dominated by transitions from the HOMO−1 or the HOMO−2 to the LUMO or higher vacant orbitals, typically, HOMO−1/2 → LUMO+2/3. Considering the different localizations of both HOMOs on the Fe-atom and the adjacent Cp ring (see above and Fig. S20–37†), mixed interactions were found to form the LE band of **2a** and **5a–9a**. The HE bands of compounds **1a–9a** are formed by the HOMO → LUMO and eventually the HOMO−2 → LUMO transitions and again both Fe → Py and Cp → Py interactions were identified. Hence, ferrocene push–pull molecules **a** bearing weak pyridine acceptor do not obey the aforementioned model on two separate interactions resulting in two bands. On the contrary, the spectra of pyridinium chromophores **1b–9b** feature bathochromically and

Table 2 DFT calculated properties of chromophores **1a–9a** and **1b–9b**[a]

Comp.	E_{HOMO-3} [eV]	E_{HOMO-2} [eV]	E_{HOMO-1} [eV]	E_{HOMO} [eV]	E_{LUMO} [eV]	E_{LUMO+1} [eV]	E_{LUMO+2} [eV]	E_{LUMO+3} [eV]	μ [D]	$\lambda_{max}^{HE/LE}$ [nm (eV)]	β $(-2\omega, \omega, \omega)$[b] [$\times 10^{-30}$ esu]
1a	−6.71	−6.52	−5.77	−5.73	−1.49	−0.77	−0.56	−0.45	4.6	324 (3.83)/—	7
2a	−6.54	−6.25	−5.74	−5.64	−1.93	−0.72	−0.59	−0.51	5.3	362 (3.43)/592 (2.09)	31
3a	−6.66	−6.47	−5.83	−5.77	−1.91	−0.84	−0.69	−0.63	5.2	342 (3.63)/—	28
4a	−6.50	−6.26	−5.69	−5.62	−1.79	−0.85	−0.66	−0.62	4.8	352 (3.52)/—	33
5a	−6.49	−6.02	−5.69	−5.58	−2.23	−0.84	−0.75	−0.68	5.7	382 (3.25)/580 (2.14)	124
6a	−6.52	−6.17	−5.72	−5.63	−2.19	−0.95	−0.87	−0.76	5.9	382 (3.25)/589 (2.10)	101
7a	−6.54	−6.06	−5.75	−5.60	−2.06	−0.85	−0.65	−0.60	5.6	385 (3.22)/591 (2.10)	45
8a	−6.53	−5.91	−5.75	−5.50	−2.31	−0.95	−0.72	−0.60	6.5	420 (2.95)/598 (2.07)	137
9a	−6.56	−6.02	−5.77	−5.60	−2.27	−1.06	−0.85	−0.62	6.4	393 (3.15)/593 (2.09)	118
1b	−7.14	−6.81	−6.07	−6.06	−2.71	−1.71	−0.94	−0.82	12.5	374 (3.32)/618 (2.00)	24
2b	−6.81	−6.59	−5.97	−5.89	−2.98	−1.66	−0.90	−0.78	17.6	387 (3.20)/642 (1.93)	107
3b	−6.97	−6.74	−6.04	−6.02	−3.10	−1.73	−0.94	−0.89	18.4	375 (3.31)/624 (1.99)	176
4b	−6.64	−6.47	−5.81	−5.75	−2.95	−1.79	−1.10	−0.90	24.1	396 (3.13)/612 (2.03)	116
5b	−6.59	−6.27	−5.80	−5.71	−3.14	−1.68	−1.39	−0.86	28.8	445 (2.79)/629 (1.97)	255
6b	−6.61	−6.39	−5.81	−5.74	−3.28	−1.84	−1.47	−1.04	29.7	445 (2.79)/640 (1.94)	4166
7b	−6.71	−6.37	−5.91	−5.80	−3.04	−1.71	−1.20	−0.75	20.5	425 (2.92)/633 (1.96)	2218
8b	−6.66	−6.14	−5.88	−5.71	−3.14	−1.63	−1.53	−0.72	25.0	467 (2.66)/642 (1.93)	503
9b	−6.68	−6.25	−5.89	−5.76	−3.22	−1.77	−1.62	−0.73	26.8	463 (2.68)/639 (1.94)	203

[a] All data were calculated at the DFT B3LYP/6-311+G(2df,p) level with acetonitrile as solvent. [b] In vacuum at 1064 nm.

hyperchromically shifted LE bands, which are mostly formed by the HOMO → LUMO transition eventually also accompanied by the transition from the HOMO−1, thus both Fe-centered orbitals. The HE band is composed of two dominant transitions – HOMO−2 → LUMO and HOMO−3 → LUMO. Hence, we can conclude that in Fc–π–Py^+ chromophores **b** two separate Fe → Py^+ and Cp → Py^+ interactions resulting in the LE and HE bands can be identified.

The first-order hyperpolarizabilities β $(-2\omega, \omega, \omega)$ were calculated for both series of chromophores (Table 2). Considering the overestimated β values of **6b**/**7b** as outliers, the calculated hyperpolarizabilities are slightly higher to those calculated for previous Fc–π–imidazole derivatives.[18a] The hyperpolarizabilities increase with enlarged and planarized π-system. For instance, β values of **1a**, **2a** and **3a** (7, 31 and 28 × 10^{-30} esu) reflect extension and planarization by adding olefinic spacer as compared to the acetylenic one. However, when interconnecting the electronegative acetylene and pyridinium moieties as in **3b**, a strong electron-withdrawing group is formed with increased hyperpolarizability to 176 × 10^{-30} esu. A comparison of **4a** and **7a** clearly illustrates a beneficial role of 2,5-thienylene over 1,4-phenylene spacers. In general, *N*-quaternized chromophores in series **b** showed enhanced nonlinearity with the largest first-order hyperpolarizability of 503 × 10^{-30} esu calculated for **8b** bearing polarizable thiophene and olefinic π-system.

Conclusion

A series of push–pull molecules with ferrocene donor, pyridine/pyridinium acceptors and systematically enlarged π-system has been designed and prepared. The synthesis involved Suzuki–Miyaura, Sonogashira or Heck cross-coupling reactions. Two chromophores were successfully crystallized and their molecular structure was confirmed by X-ray analysis. Electrochemical measurements revealed that structural tuning *via* π-system extension and *N*-quaternization principally affects the LUMO with the almost steady HOMO. The HOMO–LUMO gap of chromophores **1–9** can be tuned within a broad range of 3.01 to 1.49 eV. Two LE and HE bands were identified in the electronic absorption spectra; the latter was significantly affected by the π-system extension. The *N*-quaternization red-shifted both bands by *ca.* 30–90 nm. A diminished solvatochromism was observed for pyridine chromophores **1a–9a**, while pyridinium compounds **1b–9b** showed distinct negative solvatochromism. The performed DFT analysis corroborated the experimental observations and especially shed light on different D–A interactions seen for Fc–π–Py and Fc–π–Py^+ chromophores. The ferrocene turned out to be an electron donor with two principal charge-transfers that, based on the appended acceptor, are variously employed.

Experimental

All reagents and solvents were reagent grade and were purchased from Penta, Aldrich, and TCI and used as received. The starting ferroceneboronic acid **10**, 4-pyridinylboronic acid **11**, vinylferrocene **12**, 4-vinylpyridine **13**, ethynylferrocene **14**, 4-ethynylpyridine hydrochloride **15** and 4-iodopyridine **16** were commercially available. Compound **19** was reported previously.[18b] All cross-coupling reactions were carried out in flame-dried flasks under an argon atmosphere. Thin layer chromatography (TLC) was conducted on aluminum sheets coated with silica gel 60 F254 with visualization by a UV lamp (254 or 360 nm). Column chromatography was carried out with silica gel 60 (particle size 0.040–0.063 mm, 230–400 mesh) and

commercially available solvents. ^{1}H and ^{13}C NMR spectra were recorded on a Bruker AVANCE II/III 400/500 spectrometer (400/500 MHz or 100/125 MHz, respectively). Chemical shifts are reported in ppm relative to the signal of Me_4Si (0.00 ppm). The residual solvent signal was used as an internal reference ($CDCl_3$ 7.25 and 77.23 ppm; DMSO-d_6 2.55 and 39.52). Apparent resonance multiplicities are described as s (singlet), d (doublet), dd (doublet of doublet), and m (multiplet). ^{1}H NMR signals of pyridine, thiophene and cyclopentadienyl are denoted as Py, Th and Cp. The coupling constants, J, are reported in Hertz (Hz). High-resolution MALDI mass spectroscopy data were collected on an LTQ Orbitrap XL. Absorption spectra were measured on a UV/vis HP 8453 spectrophotometer at room temperature.

General procedure for the Suzuki–Miyaura cross-coupling (compounds 1a, 4a, 7a and 9a)

In a Schlenk flask, ferroceneboronic acid **10** (276 mg, 1.0 mmol) or 4-pyridinylboronic acid **11** (148 mg, 1.2 mmol) and corresponding halogen derivative (1.0 mmol) were dissolved in 1,2-dimethoxyethane (10 mL) or in a mixture of 1,4-dioxane/H_2O (25 mL, 4 : 1). Argon was bubbled through the solution for 10 min, whereupon $PdCl_2[Fe(PPh_3)_2]_2$ (35 mg, 0.05 mmol, 5%) along with a solution of sodium hydroxide (1 mL of 10% solution, 3 mmol) or $PdCl_2(PPh_3)_2$ (35 mg, 0.05 mmol, 5%) and K_2CO_3 (150 mg, 1.1 mmol) were added and the resulting reaction mixture was stirred at 85 °C for 12 h. The reaction mixture was diluted with water (100 mL) and extracted with CH_2Cl_2 (3 × 50 mL). The combined organic extracts were washed with water, dried over anhydrous Na_2SO_4, the solvents were evaporated *in vacuo* and the crude product was purified by column chromatography.

General procedure for the Heck cross-coupling (compounds 2a, 5a, 8a)

In a Schlenk flask, vinylferrocene **12** (424 mg, 2.0 mmol) or vinylpyridine **13** (210 mg, 2.0 mmol) and corresponding iodo derivative (2.0 mmol) were dissolved in a DMF (10 mL). Ethyldiisopropylamine (0.4 mL, 2.3 mmol) was added and argon was bubbled through the solution for 10 min, whereupon $[t\mathrm{Bu}_3\mathrm{P}]_2\mathrm{Pd}$ (50 mg, 0.1 mmol, 5%) was added and the resulting reaction mixture was stirred at 85 °C for 12 h. The reaction mixture was diluted with water (100 mL) and extracted with EtAc (3 × 50 mL). The combined organic extracts were washed with water, dried over anhydrous Na_2SO_4, the solvents were evaporated *in vacuo* and the crude product was purified by column chromatography.

General procedure for the Sonogashira cross-coupling (compounds 3a and 6a)

In a Schlenk flask, ethynylferrocene **14** (315 mg, 1.5 mmol) or ethynylpyridine hydrochloride **15** (210 mg, 1.5 mmol) and corresponding iodo derivate (1.0 mmol) were dissolved in a THF (15 mL). Ethyldiisopropylamine (2 mL, 11.5 mmol)) was added and argon was bubbled through the solution for 10 min, whereupon $PdCl_2(PPh_3)_2$ (35 mg, 0.05 mmol, 5%) and copper iodide (15 mg, 0.025 mmol, 2.5%) were added and the resulting reaction mixture was stirred at 60 °C for 12 h. The reaction mixture was diluted with water (100 mL) and extracted with CH_2Cl_2 (3 × 50 mL). The combined organic extracts were dried over anhydrous Na_2SO_4, the solvents were evaporated *in vacuo* and the crude product was purified by column chromatography.

General procedure for quaternization (compounds 1b–9b)

In a 10 mL flask, ferrocenylpyridine derivates **1a–9a** (0.3 mmol) and methyliodide (6 mL, 9.7 mmol) were stirred under reflux for 1 h. The reaction mixture was cooled to 25 °C and the formed quaternary salt was filtered off and washed with ether.

4-Ferrocenylpyridine (1a). The title compound was prepared from **10** (230 mg, 1.0 mmol) and **16** (246 mg, 1.2 mmol) following the general method for the Suzuki–Miyaura reaction (DME, $PdCl_2[Fe(PPh_3)_2]_2$, NaOH solution). The crude product was purified by column chromatography (SiO_2, CH_2Cl_2/EtAc, 5 : 2). Yield: 126 mg (48%); orange solid; R_f = 0.20 (SiO_2; CH_2Cl_2/EtAc, 5 : 2); mp 139–140 °C; ^{1}H NMR (400 MHz, $CDCl_3$, 25 °C): δ = 4.03 (s, 5H; Cp), 4.42 (bs, 2H; Cp), 4.72 (bs, 2H, Cp), 7.33 (d, J = 4 Hz, 2H; PyH), 8.50 ppm (bs, 2H; PyH); ^{13}C NMR (100 MHz, $CDCl_3$, 25 °C): δ = 149.77, 148.98, 120.95, 81.09, 70.48, 70.18, 67.06 ppm; FTIR (HATR): $\tilde{\nu}$ = 3032, 1590, 1414, 1104, 996, 821, 484 cm^{-1}; HR-FT-MALDI-MS (DHB): m/z calcd for $C_{15}H_{13}FeN$ $[M + H]^+$ 264.04757; found: 264.04713.

(*E*)-4-(2′-Ferrocenylethenyl)pyridine (2a). The title compound was prepared from **12** (424 mg, 2.0 mmol) and **16** (410 mg, 2.0 mmol) following the general method for the Heck reaction. The crude product was purified by column chromatography (SiO_2, CH_2Cl_2–EtAc, 5 : 2). Yield: 352 mg (61%); dark red solid; R_f = 0.35 (SiO_2; CH_2Cl_2–EtAc, 5 : 2); mp 154–156 °C; ^{1}H NMR (500 MHz, $CDCl_3$, 25 °C): δ = 4.14 (s, 5H; Cp), 4.35 (bs, 2H; Cp), 4.49 (bs, 2H; Cp), 6.58 (d, J = 16 Hz, 1H; CH), 7.12 (d, J = 16 Hz, 1H; CH), 7.28 (bs, 2H; Py), 8.51 ppm (bs, 2H; Py); ^{13}C NMR (125 MHz, $CDCl_3$, 25 °C): δ = 149.90, 145.51, 132.94, 123.05, 120.36, 81.60, 70.06, 69.53, 67.61 ppm; FTIR (HATR): $\tilde{\nu}$ = 3080, 1625, 1585, 1410, 1191, 805, 476 cm^{-1}; HR-FT-MALDI-MS (DHB): m/z calcd for $C_{17}H_{15}FeN$ $[M + H]^+$ 290.06322; found: 290.06265.

4-Ferrocenylethynylpyridine (3a). The title compound was prepared from **14** (315 mg, 1.5 mmol) and **16** (205 mg, 1.0 mmol) following the general method for the Sonogashira reaction. The crude product was purified by column chromatography (SiO_2, CH_2Cl_2/EtAc, 5 : 2). Yield: 195 mg (68%); dark red solid; R_f = 0.45 (SiO_2; CH_2Cl_2/EtAc, 5 : 2); mp 154–156 °C; ^{1}H NMR (500 MHz, $CDCl_3$, 25 °C): δ = 4.24 (s, 5H; Cp), 4.29 (bs, 2H; Cp), 4.53 (bs, 2H, Cp), 7.33 (bs, 2H; Py), 8.57 ppm (bs, 2H; Py); ^{13}C NMR (125 MHz, $CDCl_3$, 25 °C): δ = 149.76, 132.25, 125.52, 94.32, 83.54, 71.89, 70.23, 69.58, 63.71 ppm; FTIR (HATR): $\tilde{\nu}$ = 3062, 2206, 1588, 1407, 1168, 812, 482 cm^{-1}; HR-FT-MALDI-MS (DHB): m/z calcd for $C_{17}H_{13}FeN$ $[M + H]^+$ 288.04757; found: 288.04578.

4-(4′-Ferrocenylphenyl)pyridine (4a). The title compound was prepared from **11** (148 mg, 1.2 mmol) and **18** (388 mg, 1.0 mmol) following the general method for the Suzuki–Miyaura reaction (1,4-dioxane/H_2O, $PdCl_2(PPh_3)_2$, K_2CO_3). The crude product was purified by column chromatography (SiO_2, CH_2Cl_2/EtAc, 5 : 2). Yield: 180 mg (53%); orange-red solid; R_f = 0.25

(SiO_2; CH_2Cl_2/EtAc, 5 : 2); mp 218–219 °C; ^{1}H NMR (400 MHz, $CDCl_3$, 25 °C): δ = 4.06 (s, 5H; Cp), 4.36 (bs, 2H; Cp), 4.69 (bs, 2H; Cp), 7.54–7.57 (m, 6H; ArH, Py), 8.66 ppm (bs, 2H; Py); ^{13}C NMR (125 MHz, $CDCl_3$, 25 °C): δ = 150.21, 148.04, 140.86, 135.18, 126.91, 126.66, 84.09, 69.73, 69.39, 66.63 ppm; FTIR (HATR): $\tilde{\nu}$ = 3029, 1588, 1403, 1230, 994, 806, 491 cm^{-1}; HR-FT-MALDI-MS (DHB): *m*/*z* calcd for $C_{21}H_{17}FeN$ $[M + H]^+$ 340.07887; found: 340.07854.

(*E*)-4-(4′-Ferrocenylstyryl)pyridine (5a). The title compound was prepared from **13** (210 mg, 2.0 mmol) and **18** (776 mg, 2.0 mmol) following the general method for the Heck reaction. The crude product was purified by column chromatography (SiO_2, CH_2Cl_2/EtAc, 5 : 2). Yield: 387 mg (53%); red solid; R_f = 0.40 (SiO_2; CH_2Cl_2/EtAc, 5 : 2); mp 236–238 °C; ^{1}H NMR (500 MHz, $CDCl_3$, 25 °C): δ = 4.05 (s, 5H; Cp), 4.36 (bs, 2H; Cp), 4.69 (bs, 2H; Cp), 7.01 (d, J = 16 Hz, 1H; CH), 7.29 (d, J = 16 Hz, 1H; CH), 7.40 (bs, 2H; Py), 7.45–7.49 (m, 4H; ArH), 8.59 ppm (bs, 2H; Py); ^{13}C NMR (125 MHz, $CDCl_3$, 25 °C): δ = 150.15, 145.11, 140.62, 133.72, 133.30, 127.27, 126.45, 124.97, 120.96, 84.48, 69.95, 69.49, 66.65 ppm; FTIR (HATR): $\tilde{\nu}$ = 3020, 1582, 1411, 1276, 1106, 826, 475 cm^{-1}; HR-FT-MALDI-MS (DHB): *m*/*z* calcd for $C_{23}H_{19}FeN$ $[M + H]^+$ 366.09452; found: 366.09330.

4-((4′-Ferrocenylphenyl)ethynyl)pyridine (6a). The title compound was prepared from **15** (208 mg, 1.5 mmol) and **18** (388 mg, 1.0 mmol) following the general method for the Sonogashira reaction. The crude product was purified by column chromatography (SiO_2, CH_2Cl_2/EtAc, 5 : 2). Yield: 290 mg (80%); red solid; R_f = 0.45 (SiO_2; CH_2Cl_2/EtAc, 5 : 2); mp 225–226 °C; ^{1}H NMR (500 MHz, $CDCl_3$, 25 °C): δ = 4.05 (s, 5H; Cp), 4.38 (bs, 2H; Cp), 4.68 (bs, 2H; Cp), 7.39 (bs, 2H; Py), 7.46 (bs, 4H; ArH), 8.60 ppm (bs, 2H; Py); ^{13}C NMR (125 MHz, $CDCl_3$, 25 °C): δ = 149.72, 141.34, 132.09, 131.97, 126.03, 125.67, 119.11, 94.84, 86.87, 83.91, 69.91, 69.72, 66.74 ppm; FTIR (HATR): $\tilde{\nu}$ = 3082, 2212, 1581, 1407, 1105, 816, 481 cm^{-1}; HR-FT-MALDI-MS (DHB): *m*/*z* calcd for $C_{23}H_{17}FeN$ $[M]^+$ 363.07104; found: 363.07083.

4-(5′-Ferrocenylthiophen-2-yl)pyridine (7a). The title compound was prepared from **11** (148 mg, 1.2 mmol) and **19** (394 mg, 1.0 mmol) following the general method for the Suzuki–Miyaura reaction (1,4-dioxane/H_2O, $PdCl_2(PPh_3)_2$, K_2CO_3). The crude product was purified by column chromatography (SiO_2, CH_2Cl_2/EtAc, 5 : 2). Yield: 221 mg (64%); dark red solid; R_f = 0.30 (SiO_2; CH_2Cl_2/EtAc, 5 : 2); mp 187–188 °C; ^{1}H NMR (500 MHz, $CDCl_3$, 25 °C): δ = 4.11 (s, 5H; Cp), 4.34 (bs, 2H; Cp), 4.61 (bs, 2H; Cp), 7.01 (d, J = 3 Hz, 1H; ThH), 7.34 (d, J = 3 Hz, 1H; ThH), 7.45 (bs, 2H; Py), 8.57 ppm (bs, 2H; Py); ^{13}C NMR (125 MHz, $CDCl_3$, 25 °C): δ = 150.38, 146.34, 141.64, 137.96, 126.00, 123.51, 119.35, 79.13, 70.31, 69.31, 67.19 ppm; FTIR (HATR): $\tilde{\nu}$ = 3075, 1584, 1409, 987, 799, 485 cm^{-1}; HR-FT-MALDI-MS (DHB): *m*/*z* calcd for $C_{19}H_{15}FeNS$ $[M + H]^+$ 346.03529; found: 346.03502.

(*E*)-4-(2′-(5″-Ferrocenylthiophen-2″-yl)ethenyl)pyridine (8a). The title compound was prepared from **13** (210 mg, 2.0 mmol) and **19** (788 mg, 2.0 mmol) following the general method for the Heck reaction. The crude product was purified by column chromatography (SiO_2, CH_2Cl_2/EtAc, 5 : 2). Yield: 441 mg (64%); dark red solid; R_f = 0.35 (SiO_2; CH_2Cl_2/EtAc, 5 : 2); mp 164–165 °C; ^{1}H NMR (400 MHz, $CDCl_3$, 25 °C): δ = 4.11 (s, 5H; Cp), 4.33 (bs, 2H; Cp), 4.59 (bs, 2H; Cp), 6.72 (d, J = 16 Hz, 1H; CH), 6.91–6.95 (m, 2H; CH, Th), 7.31–7.38 (m, 3H; Th, Py), 8.58 ppm (bs, 2H; Py); ^{13}C NMR (125 MHz, $CDCl_3$, 25 °C): δ = 150.24, 145.08, 144.70, 139.10, 129.25, 126.52, 123.98, 122.86, 120.68, 79.37, 70.29, 69.28, 67.12 ppm; FTIR (HATR): $\tilde{\nu}$ = 3077, 1587, 1410, 1032, 942, 802, 477 cm^{-1}; HR-FT-MALDI-MS (DHB): *m*/*z* calcd for $C_{21}H_{17}FeNS$ $[M + H]^+$ 372.05094; found: 372.05046.

4-((5′-Ferrocenylthiophen-2′-yl)ethynyl)pyridine (9a). The title compound was prepared from **10** (230 mg, 1.0 mmol) and **17** (318 mg, 1.2 mmol) following the general method for the Suzuki–Miyaura reaction (DME, $PdCl_2[Fe(PPh_3)_2]_2$, NaOH solution). The crude product was purified by column chromatography (SiO_2, CH_2Cl_2/EtAc, 5 : 2). Yield: 181 mg (49%); orange red solid; R_f = 0.45 (SiO_2; CH_2Cl_2/EtAc, 5 : 2); mp 149–150 °C; ^{1}H NMR (500 MHz, $CDCl_3$, 25 °C): δ = 4.09 (s, 5H; Cp), 4.32 (t, J = 2 Hz, 2H; Cp), 4.58 (t, J = 2 Hz, 2H; Cp), 6.90 (d, J = 4 Hz, 1H; Th), 7.15 (d, J = 4 Hz, 1H; Th), 7.35 (bs, 2H; Py), 8.58 ppm (bs, 2H; Py); ^{13}C NMR (125 MHz, $CDCl_3$, 25 °C): δ = 149.68, 147.89, 134.19, 131.63, 125.14, 122.37, 118.80, 90.84, 88.54, 78.70, 70.35, 69.41, 67.28 ppm; FTIR (HATR): $\tilde{\nu}$ = 3073, 2183, 1588, 1407, 1029, 803, 500 cm^{-1}; HR-FT-MALDI-MS (DHB): *m*/*z* calcd for $C_{21}H_{15}FeNS$ $[M + H]^+$ 370.03529; found: 370.03484.

1-Methyl-4-ferrocenylpyridinium iodide (1b). The title compound was prepared from **1a** (79 mg) following the general method for the quaternization. Yield: 119 mg (98%); dark red solid; ^{1}H NMR (500 MHz, DMSO-d_6, 25 °C): δ = 4.15–4.23 (m, 8H; Cp, CH_3), 4.79 (bs, 2H; Cp), 5.29 (bs, 2H, Cp), 8.07 (bs, 2H; Py), 8.66 ppm (bs, 2H; Py); ^{13}C NMR (125 MHz, DMSO-d_6, 25 °C): δ = 159.73, 144.52, 122.61, 76.55, 73.84, 71.16, 69.34, 46.92 ppm; FTIR (HATR): $\tilde{\nu}$ = 3009, 1633, 1528, 1187, 998, 831, 482 cm^{-1}; HR-FT-MALDI-MS (DHB): *m*/*z* calcd for $C_{16}H_{16}FeN$ $[M]^+$ 278.06322; found: 278.06257.

1-Methyl-(*E*)-4-(2′-ferrocenylethenyl)pyridinium iodide (2b). The title compound was prepared from **2a** (87 mg) following the general method for the quaternization. Yield: 127 mg (98%); black solid; ^{1}H NMR (500 MHz, DMSO-d_6, 25 °C): δ = 4.22 (s, 3H; CH_3), 4.27 (s, 5H; Cp), 4.65 (bs, 2H; Cp), 4.79 (bs, 2H; Cp), 7.02 (d, J = 16 Hz, 1H; CH), 7.93 (d, J = 16 Hz, 1H; CH), 8.11 (d, J = 6 Hz, 2H; Py), 8.79 ppm (d, J = 6 Hz, 2H; Py); ^{13}C NMR (125 MHz, DMSO-d_6, 25 °C): δ = 152.89, 145.18, 143.55, 122.75, 120.25, 80.49, 71.96, 70.14, 69.14, 47.04 ppm; FTIR (HATR): $\tilde{\nu}$ = 3012, 1643, 1597, 1474, 1176, 836, 485 cm^{-1}; HR-FT-MALDI-MS (DHB): *m*/*z* calcd for $C_{18}H_{18}FeN$ $[M]^+$ 304.07887; found: 304.07818.

1-Methyl-4-ferrocenylethynylpyridinium iodide (3b). The title compound was prepared from **3a** (86 mg) following the general method for the quaternization. Yield: 122 mg (95%); dark red solid; ^{1}H NMR (500 MHz, DMSO-d_6, 25 °C): δ = 4.31 (s, 3H; CH_3), 4.39 (s, 5H; Cp), 4.62 (bs, 2H; Cp), 4.80 (bs, 2H, Cp), 8.17 (bs, 2H; Py), 8.96 ppm (bs, 2H; Py); ^{13}C NMR (125 MHz, DMSO-d_6, 25 °C): δ = 145.70, 138.29, 128.61, 105.76, 83.42, 72.89, 71.52, 70.77, 61.15, 47.96 ppm; FTIR (HATR): $\tilde{\nu}$ = 3064, 2190, 1629, 1516, 1159, 820, 477 cm^{-1}; HR-FT-MALDI-MS (DHB): *m*/*z* calcd for $C_{18}H_{16}FeN$ $[M]^+$ 302.06322; found: 302.06212.

1-Methyl-4-(4′-ferrocenylphenyl)pyridinium iodide (4b). The title compound was prepared from **4a** (102 mg) following the general method for the quaternization. Yield: 124 mg (86%); orange-red solid; ^{1}H NMR (500 MHz, DMSO-d_6, 25 °C): δ = 4.10 (s, 5H; Cp), 4.36 (s, 3H; CH_3), 4.53 (bs, 2H; Cp), 5.04 (bs, 2H; Cp), 7.83 (d, J = 9 Hz, 2H; ArH), 8.08 (d, J = 9 Hz, 2H; ArH), 8.57 (d, J = 7 Hz, 2H; Py), 9.01 ppm (d, J = 7 Hz, 2H; Py); ^{13}C NMR (125 MHz, DMSO-d_6, 25 °C): δ = 154.24, 145.82, 144.98, 130.66, 128.59, 127.11, 123.69, 82.90, 70.47, 70.10, 67.36, 47.34 ppm; FTIR (HATR): $\tilde{\nu}$ = 3062, 1601, 1508, 1234, 810, 503 cm^{-1}; HR-FT-MALDI-MS (DHB): m/z calcd for $C_{22}H_{20}FeN$ $[M]^+$ 354.09452; found: 354.09429.

1-Methyl-(*E*)-4-(4′-ferrocenylstyryl)pyridinium iodide (5b). The title compound was prepared from **5a** (110 mg) following the general method for the quaternization. Yield: 132 mg (87%); red solid; ^{1}H NMR (500 MHz, DMSO-d_6, 25 °C): δ = 4.08 (s, 5H; Cp), δ = 4.29 (s, 3H; CH_3), 4.49 (bs, 2H; Cp), 4.96 (bs, 2H; Cp), 7.55 (d, J = 16 Hz, 1H; CH), 7.69–7.74 (m, 4H; ArH), 8.05 (d, J = 16 Hz, 2H; CH), 8.26 (d, J = 7 Hz, 2H; Py), 8.89 ppm (d, J = 7 Hz, 2H; Py); ^{13}C NMR (125 MHz, DMSO-d_6, 25 °C): δ = 153.12, 145.46, 142.80, 141.15, 132.97, 128.82, 126.69, 123.70, 122.43, 83.77, 70.14, 70.03, 67.06, 47.29 ppm; FTIR (HATR): $\tilde{\nu}$ = 3013, 1597, 1520, 1180, 977, 821, 490 cm^{-1}; HR-FT-MALDI-MS (DHB): m/z calcd for $C_{24}H_{22}FeN$ $[M]^+$ 380.11017; found: 380.10970.

1-Methyl-4-((4′-ferrocenylphenyl)ethynyl)pyridinium iodide (6b). The title compound was prepared from **6a** (109 mg) following the general method for the quaternization. Yield: 138 mg (91%); orange-red solid; ^{1}H NMR (500 MHz, DMSO-d_6, 25 °C): δ = 4.01 (s, 5H; Cp), 4.36 (s, 3H; CH_3), 4.52 (bs, 2H; Cp), 4.98 (bs, 2H; Cp), 7.67 (d, J = 8 Hz, 2H; ArH), 7.74 (d, J = 8 Hz, 2H; ArH), 8.28 (d, J = 7 Hz, 2H; Py), 9.03 ppm (d, J = 7 Hz, 2H; Py); ^{13}C NMR (125 MHz, DMSO-d_6, 25 °C): δ = 145.95, 143.79, 138.96, 133.04, 129.12, 126.62, 116.98, 103.58, 86.31, 83.09, 70.44, 70.11, 67.25, 48.15 ppm; FTIR (HATR): $\tilde{\nu}$ = 2991, 2213, 1627, 1527, 1140, 821, 486 cm^{-1}; HR-FT-MALDI-MS (DHB): m/z calcd for $C_{24}H_{20}FeN$ $[M]^+$ 378.09452; found: 378.09409.

1-Methyl-4-(5′-ferrocenylthiophen-2-yl)pyridinium iodide (7b). The title compound was prepared from **7a** (104 mg) following the general method for the quaternization. Yield: 137 mg (94%); dark red solid; ^{1}H NMR (500 MHz, DMSO-d_6, 25 °C): δ = 4.17–4.24 (m, 8H; Cp, CH_3), 4.56 (bs, 2H; Cp), 4.90 (bs, 2H; Cp), 7.48 (bs, 1H; Th), 8.17 (bs, 1H; Th), 8.27 (bs, 2H; Py), 8.83 ppm (bs, 2H; Py); ^{13}C NMR (125 MHz, DMSO-d_6, 25 °C): δ = 152.40, 146.88, 144.72, 132.99, 132.91, 125.13, 120.50, 76.89, 69.84, 69.78, 67.08, 46.20 ppm; FTIR (HATR): $\tilde{\nu}$ = 3022, 1631, 1417, 1187, 812, 488 cm^{-1}; HR-FT-MALDI-MS (DHB): m/z calcd for $C_{20}H_{18}FeNS$ $[M]^+$ 360.05094; found: 360.05045.

1-Methyl-(*E*)-4-(2′-(5″-ferrocenylthiophen-2″-yl)ethenyl)pyridinium iodide (8b). The title compound was prepared from **8a** (111 mg) following the general method for the quaternization. Yield: 145 mg (94%); dark red solid; ^{1}H NMR (500 MHz, DMSO-d_6, 25 °C): δ = 4.17 (s, 5H; Cp), 4.25 (s, 3H; CH_3), 4.52 (bs, 2H; Cp), 4.84 (bs, 2H; Cp), 7.11 (d, J = 16 Hz, 1H; CH), 7.29 (d, J = 4 Hz, 1H; Th), 7.39 (d, J = 4 Hz, 1H; Th), 8.18–8.23 (m, 3H, CH, Py), 8.82 ppm (d, J = 7 Hz, 2H; Py); ^{13}C NMR (125 MHz, DMSO-d_6, 25 °C): δ = 152.85, 148.86, 145.22, 138.23, 134.46, 133.88, 124.62, 123.17, 120.79, 79.63, 70.55, 70.22, 67.62, 47.15 ppm; FTIR (HATR): $\tilde{\nu}$ = 3014, 1596, 1417, 1184, 961, 811, 483 cm^{-1}; HR-FT-MALDI-MS (DHB): m/z calcd for $C_{22}H_{20}FeNS$ $[M]^+$ 386.06659; found: 386.06630.

1-Methyl-4-((5′-ferrocenylthiophen-2′-yl)ethynyl)pyridinium iodide (9b). The title compound was prepared from **9a** (111 mg) following the general method for the quaternization. Yield: 127 mg (83%); dark red solid; ^{1}H NMR (500 MHz, DMSO-d_6, 25 °C): δ = 4.09 (s, 5H; Cp), 4.26 (s, 3H; CH_3), 4.46 (bs, 2H; Cp), 4.81 (bs, 2H; Cp), 7.27 (bs, 1H; Th), 7.54 (bs, 1H; Th), 8.16 (bs, 2H; Py), 8.92 ppm (bs, 2H; Py); ^{13}C NMR (125 MHz, DMSO-d_6, 25 °C): δ = 151.70, 145.80, 138.50, 138.23, 128.25, 124.30, 116.16, 97.56, 91.00, 77.82, 70.63, 70.35, 67.87, 48.04 ppm; FTIR (HATR): $\tilde{\nu}$ = 3058, 2184, 1629, 1467, 1210, 813, 485 cm^{-1}; HR-FT-MALDI-MS (DHB): m/z calcd for $C_{22}H_{18}FeNS$ $[M]^+$ 384.05094; found: 384.05048.

Author contributions

Funding acquisition: FB; investigation: JK, MK, OP, ZR; methodology: JK, FB; project administration: FB; writing – original draft: FB; writing – review & editing: FB.

Conflicts of interest

There are no conflicts to declare.

Acknowledgements

The work has been supported from European Regional development Fund-Project "Organic redox couple based batteries for energetics of traditional and renewable resources (ORGBAT)", No. CZ.02.1.01/0.0/0.0/16_025/0007445.

References

1 F. Bureš, *RSC Adv.*, 2014, **4**, 58826.
2 (*a*) Q. Wei, N. Fei, A. Islam, T. Lei, L. Hong, R. Peng, X. Fan, L. Chen, P. Gao and Z. Ge, *Adv. Opt. Mater.*, 2018, **6**, 1800512; (*b*) S. S. Swayamprabha, D. K. Dubey, Shahnawaz, R. A. K. Yadav, M. R. Nagar, A. Sharma, F.-C. Tung and J.-H. Jou, *Adv. Sci.*, 2021, **8**, 2002254.
3 (*a*) Z. A. Lamport, H. F. Haneef, S. Anand, M. Waldrip and O. D. Jurchescu, *J. Appl. Phys.*, 2018, **124**, 071101; (*b*) S. Riera-Galindo, F. Leonardi, R. Pfattner and M. Mas-Torrent, *Adv. Mater. Technol.*, 2019, **4**, 1900104.
4 O. Doat, B. H. Barboza, A. Batagin-Neto, D. Bégué and R. C. Hiorns, *Polym. Int.*, 2021, DOI: 10.1002/pi.6280.
5 M. Yahya, A. Bouziani, C. Ocak, Z. Seferoğlu and M. Sillanpää, *Dyes Pigm.*, 2021, **192**, 109227.
6 (*a*) C. W. Ghanavatkar, V. R. Mishra and N. Sekar, *Dyes Pigm.*, 2021, **191**, 109367; (*b*) J. Liu, C. Ouyang, F. Huo, W. He and A. Cao, *Dyes Pigm.*, 2020, **181**, 108509.
7 M. Klikar, P. Solanke, J. Tydlitát and F. Bureš, *Chem. Rec.*, 2016, **16**, 1886.
8 (*a*) P. Solanke, S. Achelle, N. Cabon, O. Pytela, A. Barsella, B. Caro, F. Robin-le Guen, J. Podlesný, M. KLikar and

F. Bureš, *Dyes Pigm.*, 2016, **134**, 129; (*b*) J. Podlesný, O. Pytela, M. Klikar, V. Jelínková, I. V. Kityk, K. Ozga, J. Jedryka, M. Rudysh and F. Bureš, *Org. Biomol. Chem.*, 2019, **17**, 3623; (*c*) P. Ledwon, *Org. Electron.*, 2019, **75**, 105422; (*d*) M. Klikar, V. Jelínková, Z. Růžičková, T. Mikysek, O. Pytela, M. Ludwig and F. Bureš, *Eur. J. Org. Chem.*, 2017, 2764; (*e*) J. Kulhánek and F. Bureš, *Beilstein J. Org. Chem.*, 2012, **8**, 25; (*f*) E. Novotná, I. V. Kityk, O. Pytela, F. Bureš, M. Ludwig, M. Klikar, K. Ozga and J. Jedryka, *ChemPlusChem*, 2020, **85**, 1549.

9 S. Kaur, M. Kaur, P. Kaur, K. Clays and K. Singh, *Coord. Chem. Rev.*, 2017, **343**, 185.

10 D. Brunel, G. Noirbent and F. Dumur, *Dyes Pigm.*, 2019, **170**, 107611.

11 S.-I. Kato and F. Diederich, *Chem. Commun.*, 2010, **46**, 1994.

12 P. Kaur, M. Kaur, G. Depotter, S. V. Cleuvenbergen, I. Asselberghs, K. Clays and K. Singh, *J. Mater. Chem.*, 2012, **22**, 10597.

13 F. Bureš, D. Cvejn, K. Melánová, L. Beneš, J. Svoboda, V. Zima, O. Pytela, T. Mikysek, Z. Růžičková, I. V. Kityk, A. Wojciechowski and N. AlZayed, *J. Mater. Chem. C*, 2016, **4**, 468.

14 (*a*) J. Rajput, J. R. Moss, A. T. Hutton, D. T. Hendricks, C. E. Arendse and C. Imrie, *J. Organomet. Chem.*, 2004, **689**, 1553; (*b*) S.-S. Sun, D. T. Tran, O. S. Odongo and A. J. Lees, *Inorg. Chem.*, 2002, **41**, 132; (*c*) C. Mu, S. W. Chang, K. E. Prosser, A. W. Y. Leung, S. Santacruz, T. Jang, J. R. Thompson, D. T. T. Yapp, J. J. Warren, M. B. Bally, T. V. Beischlag and C. J. Walsby, *Inorg. Chem.*, 2016, **55**, 177; (*d*) T. Romero, R. A. Orenes, A. Espinosa, A. Tárraga and P. Molina, *Inorg. Chem.*, 2011, **50**, 8214; (*e*) J. D. Carr, S. J. Coles, M. B. Hursthouse and J. H. R. Tucker, *J. Organomet. Chem.*, 2001, **637–639**, 304.

15 (*a*) B. López-Mayorga, C. I. Sandoval-Chávez, P. Carreón-Castro, V. M. Ugalde-Saldívar, F. Cortés-Guzmán, J. G. López-Cortés and M. C. Ortega-Alfaro, *New J. Chem.*, 2018, **42**, 6101; (*b*) A. D. Antuf'eva, M. V. Dmitriev, O. A. Maiorova, I. G. Mokrushin, A. R. Galeev, E. V. Shklyaeva and G. G. Abashev, *Russ. J. Org. Chem.*, 2018, **54**, 1350; (*c*) S. Sakanishi, D. A. Bardwell, S. Couchman, J. C. Jefery, J. A. McCleverty and M. D. Ward, *J. Organomet. Chem.*, 1997, **528**, 35; (*d*) G. Podolan, L. Hettmanczyk, P. Hommes, B. Sarkar and H.-U. Reissig, *Eur. J. Org. Chem.*, 2015, 7317.

16 (*a*) R. J. Durand, S. Achelle, S. Gauthier, N. Cabon, M. Ducamp, S. Kahlal, J.-Y. Saillard, A. Barsella and F. Robin-Le Guen, *Dyes Pigm.*, 2018, **155**, 68; (*b*) F. Yang, X.-L. Xu, Y.-H. Gong, W.-W. Qiu, Z.-R. Sun, J.-W. Zhou, P. Audebert and J. Tang, *Tetrahedron*, 2007, **63**, 9188; (*c*) J. A. Mata, E. Peris, I. Asselberghs, R. V. Boxel and A. Persoons, *New J. Chem.*, 2001, **25**, 1043; (*d*) J. A. Mata, S. Uriel, R. Llusar and E. Peris, *Organometallics*, 2000, **19**, 3797.

17 J. Ma, Y. Zhai, J. Chen, X. Zhou, W. Shi, J. Zhang, G. Li and H. wei Hou, *Tetrahedron*, 2020, **76**, 131054.

18 (*a*) J. Kulhánek, F. Bureš, W. Kuznik, I. V. Kityk, T. Mikysek and A. Růžička, *Chem.–Asian J.*, 2013, **8**, 465; (*b*) J. Kulhánek, F. Bureš, J. Opršal, W. Kuznik, T. Mikysek and A. Růžička, *Asian J. Org. Chem.*, 2013, **2**, 422.

19 S. M. Delgado-Rivera, G. E. Peréz-Ortiz, A. Molina-Villarino, F. Morales-Fontán, L. M. García-Santos, A. M. González-Albó, A. R. Guadalupe and I. Montes-González, *Inorg. Chim. Acta*, 2017, **468**, 245.

20 (*a*) C. W. Bird, *Tetrahedron*, 1986, **42**, 89; (*b*) C. W. Bird, *Tetrahedron*, 1985, **41**, 1409.

21 P. Solanke, F. Bureš, O. Pytela, M. Klikar, T. Mikysek, L. Mager, A. Barsella and Z. Růžičková, *Eur. J. Org. Chem.*, 2015, 5339.

22 (*a*) J. Kruszewski and T. M. Krygowski, *Tetrahedron Lett.*, 1972, **36**, 3839; (*b*) T. M. Krygowski, H. Szatylowicz, O. A. Stasyuk, J. Dominikowska and M. Palusiak, *Chem. Rev.*, 2014, **114**, 6383.

23 J. Kulhánek, F. Bureš, J. Opršal, W. Kuznik, T. Mikysek and A. Růžička, *Asian J. Org. Chem.*, 2013, **2**, 422.

24 A. Isse and A. A. Gennaro, *J. Phys. Chem. B*, 2010, **114**, 7894.

25 D. T. Sawyer, A. Sobkowiak and J. L. Roberts in *Electrochemistry for Chemists*, Wiley-Intersience, 2nd edn, 1995.

26 S. Barlow, H. E. Bunting, C. Ringham, J. C. Green, G. U. Bublitz, S. G. Boxer, J. W. Perry and S. R. Marder, *J. Am. Chem. Soc.*, 1999, **121**, 3715.

27 C. Reichardt, *Solvents and Solvent Effects in Organic Chemistry*, VCH, Weinheim, 2nd edn, 1988.

28 M. J. Frisch, G. W. Trucks, H. B. Schlegel, G. E. Scuseria, M. A. Robb, J. R. Cheeseman, G. Scalmani, V. Barone, G. A. Petersson, H. Nakatsuji, X. Li, M. Caricato, A. V. Marenich, J. Bloino, B. G. Janesko, R. Gomperts, B. Mennucci, H. P. Hratchian, J. V. Ortiz, A. F. Izmaylov, J. L. Sonnenberg, D. Williams-Young, F. Ding, F. Lipparini, F. Egidi, J. Goings, B. Peng, A. Petrone, T. Henderson, D. Ranasinghe, V. G. Zakrzewski, J. Gao, N. Rega, G. Zheng, W. Liang, M. Hada, M. Ehara, K. Toyota, R. Fukuda, J. Hasegawa, M. Ishida, T. Nakajima, Y. Honda, O. Kitao, H. Nakai, T. Vreven, K. Throssell, J. A. Montgomery, Jr, J. E. Peralta, F. Ogliaro, M. J. Bearpark, J. J. Heyd, E. N. Brothers, K. N. Kudin, V. N. Staroverov, T. A. Keith, R. Kobayashi, J. Normand, K. Raghavachari, A. P. Rendell, J. C. Burant, S. S. Iyengar, J. Tomasi, M. Cossi, J. M. Millam, M. Klene, C. Adamo, R. Cammi, J. W. Ochterski, R. L. Martin, K. Morokuma, O. Farkas, J. B. Foresman and D. J. Fox, *Gaussian 16, Revision A.03*, Gaussian, Inc., Wallingford CT, 2016.